Orbital Nature of Carboionic Monoradicals Made from Diradicals

Abel Cardenas Valdivia,[a] Yasi Dai,[b] Filippo Rambaldi,[b] Joshua E. Barker,[c]
Justin J. Dressler,[c] Zheng Zhou,[d] Yikun Zhu,[d] Zheng Wei,[d] Marina A. Petrukhina,*[d]
Michael M. Haley,*[c] Fabrizia Negri,*[b] and Juan Casado*[a]

Abstract: The electronic, optical, and solid state properties of a series of monoradicals, anions and cations obtained from starting neutral diradicals have been studied. Diradicals based on *s*-indacene and indenoacenes, with benzothiophenes fused and in different orientations, feature a varying degree of diradical character in the neutral state, which is here related with the properties of the radical redox forms. The analysis of their optical features in the polymethine mono-radicals has been carried out in the framework of the molecular orbital and valence bond theories. Electronic UV-

Vis-NIR absorption, X-ray solid-state diffraction and quantum chemical calculations have been carried out. Studies of the different positive-/negative-charged species, both residing in the same skeletal π-conjugated backbone, are rare for organic molecules. The key factor for the dual stabilization is the presence of the starting diradical character that enables to indistinctively accommodate a pseudo-hole and a pseudo-electron defect with certainly small reorganization energies for ambipolar charge transport.

Introduction

The charged forms of π-conjugated molecules are the microscopic particles transported in the semiconductor component in electrical devices, in energy storage substrates, in batteries, etc.[1,2] The charged species are attractive given that they possess an odd number of π-electrons sustained on an even number of carbon sites hence with disruption of the electron/site parity of their neutral precursors. As a result, they electronically reside between even π-electron polyenes[3] and odd electron polymethines,[4] making them ideal for π-electronic studies.

Π-electron molecules preferentially stabilize positive charges over negative charges, the latter still representing a small fraction of all existing carboions.[5,6,7] Moreover, the number of molecules able to stabilize anions and cations on identical π-conjugated molecular skeletons is even smaller.[8,9]

Recently, we have been working on neutral diradicals formed by aromatic recovery of quinoidal spacers featuring a partial unpairing of the electrons from the closed-shell (CS) full-paired configuration (Scheme 1).[10–13] Diradicals, in fact, are characterized by the diradical index, y_0, which varies from 0 to 1 from CS to open-shell (OS) molecules, respectively.[14] A consequence in symmetric diradicals of the large diradical character is that the disconnected electrons become largely confined (i.e., placed in localized orbitals).

We hypothesize that OS character in the neutral diradical precursor is a key electronic aspect to stabilize radical ions of different signs. Supporting this is that most of these molecules display amphoteric electrochemical redox behavior.[15–18] In this article, we explore the redox species of several neutral diradicals, shown in Scheme 1 that consist of planar π-conjugated platforms from the family of indenofluorene[19] and its larger congeners based on fluorenofluorene[20] (**FF**) and diindenoanthracene[21] (**DIAn**). The analogues of **FF** with benzothiophene (BT) termination replacing benzene (B) and with *anti→syn* isomerization,[22,23] the so-called indenoindenodi-benzothiophenes (**IIDBTs**), are our focus. This family of diradicals spans a range of y_0 values in Scheme 1 from modestly

[a] A. C. Valdivia, Prof. J. Casado
Department of Physical Chemistry
University of Málaga
Andalucia-Tech Campus de Teatinos s/n, 29071 Málaga (Spain)
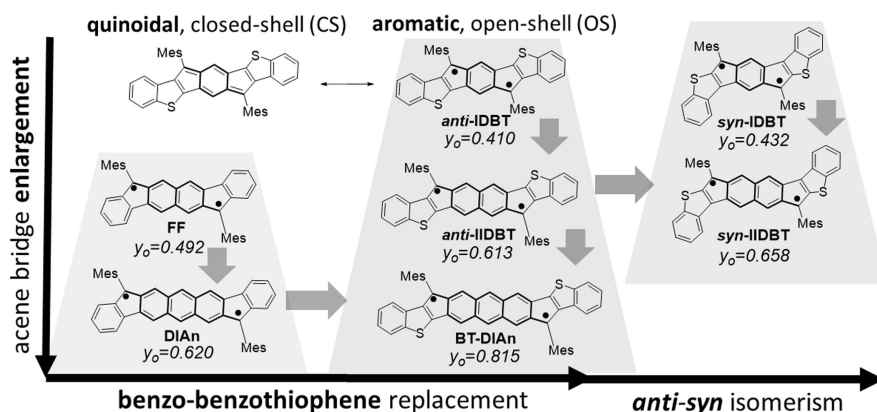E-mail: casado@uma.es

[b] Y. Dai, F. Rambaldi, Prof. F. Negri
Dipartimento di Chimica 'Giacomo Ciamician'
Università di Bologna
Via F. Selmi, 2, 40126 Bologna (Italy)
and INSTM, UdR, Bologna (Italy)
E-mail: fabrizia.negri@unibo.it

[c] Dr. J. E. Barker, Dr. J. J. Dressler, Prof. M. M. Haley
Department of Chemistry &
Biochemistry and the Materials Science Institute
University of Oregon
Eugene, Oregon 97403-1253 (USA)
E-mail: haley@uoregon.edu

[d] Dr. Z. Zhou, Y. Zhu, Dr. Z. Wei, Prof. M. A. Petrukhina
Department of Chemistry
University at Albany
State University of New York
Albany, New York 12222-0100 (USA)
E-mail: mpetrukhina@albany.edu

Chemistry–A European Journal

Research Article
doi.org/10.1002/chem.202300388

Chemistry Europe
European Chemical
Societies Publishing

Scheme 1. Neutral diradicals and PUHF/6-31G* y_0 values. In the horizontal axis, benzo-termination of **FF** and **DIAn** (B-) versus the benzothiophene substitution (BT-). In the vertical axis, molecules with increasing acene size. In the top, the quinoidal-to-aromatic (**Q-A**) conversion.

CS to pronounced OS species, which therefore allows for the exploration of the connections of the diradical strength with the structure of the generated charged species.

The opportunity to connect features of charged radicals of different signs, all having polymethine odd number of π-electrons in identical skeletons, with the underlying orbital mechanisms of electron delocalization, is the driving idea in the present work. Additionally, the principal properties of these diradicals here will be done in the context of molecular orbital (MO) description.[24,25] The MO theory is then used to analyze the evolution from diradicals to their parent radicals. A combination of experimental techniques such as UV-Vis-NIR absorption spectra obtained by spectroelectrochemistry in the anodic and cathodic branches and X-ray diffraction of crystalline sodium(I) salts of the mono- and doubly-reduced species is carried out. Quantum chemical calculations of the orbital electronic structure addressing the evaluation of intramolecular

reorganization energies for hole and electron transport are further included.

In Scheme 2, we illustrate a simple description of the orbital electronic structure of our neutral diradicals in which the unpaired electrons occupy two degenerate, singly-occupied molecular orbitals (SOMOs – SOMO1 and SOMO2). To correlate orbitals in the neutral and the charged radical molecules, in Scheme 2, we set up a common color code (same color means same orbital nature) that will be followed hereafter. Some orbital labels change from neutral to charged species, in agreement with their electron number, and the subscript (RC for radical cation, or RA for radical anion). In addition, all the orbitals are assumed to hold up to two electrons, except for the SOMO and SUMO orbitals of charged radicals. In these cases, these two different labels are used for the occupied and unoccupied orbital with the same nature (i.e., same color code), ultimately reflecting the different energy levels for α and β spin
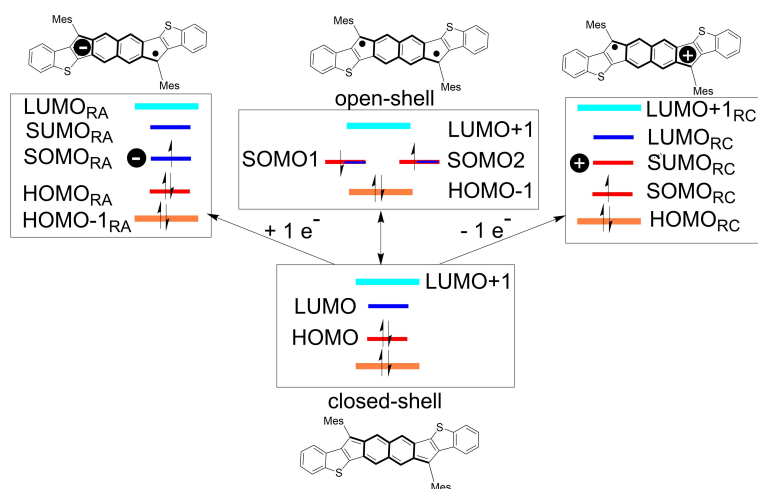
Scheme 2. Scheme and nomenclature of the gap orbitals in a diradical and in the anion (RA) and cation (RC) obtained from it. The color code correlates orbitals with similar nature in charged and neutral species. The mixed blue/red color of the SOMOs of the diradical species means that originate from mixing HOMO and LUMO of the quinoidal structure (bottom part). All orbitals are doubly occupied, except for SOMO and SUMO.

orbitals computed at the unrestricted level of theory (see below).

Results and Discussions

Crystal structures of anti-IIDBT and syn-IIDBT radical anions and dianions

The stability of the negatively charged species[26] made from these diradicals is revealed by the crystallization and x-ray characterization of the solid-state structures in the two isomers of **IIDBT**.[22,23] Synthetic details of the preparation of the crystals are summarized in Scheme S1 and the NMR spectra are shown in Figures S1 and S2. Crystal refinement details and data are given in Table S1 with ORTEP drawings in Figures S3-S5 and space-filling models in Figures S6-S8. Notably, in all crystal structures, the sodium cations are fully enveloped by 18-crown-6 ether and THF molecules, precluding direct metal binding to the anionic counterparts (Figure 1). The structural deformation of neutral *anti*-**IIDBT**[22] and *syn*-**IIDBT**[23] upon reduction (Table 1) is mainly reflected by changes of the C–C and S–C bond lengths. In neutral *syn*-**IIDBT**, the S1-C5 bond length (1.731(3) Å) is shorter than S1-C6 (1.753(4) Å), and both become slightly elongated and better equalized in the radical anion, **Na**-*syn*-**IIDBT** (avg. 1.758(5) Å) and dianion, **Na$_2$**-*syn*-**IIDBT** (avg. 1.752(8) Å). Compared to the neutral state, the bond lengths of C3-C4, C5-C12, and C13-C14 in **Na$_2$**-*syn*-**IIDBT** are elongated to 1.471(9), 1.410(10), and 1.379(9) Å, respectively; in contrast, those of C1′-C14 and C4-C5 are shortened to 1.402(9) and 1.400(10) Å, respectively.

In neutral *anti*-**IIDBT**,[22] the two S–C bonds show even more inequality (1.760(3) and 1.716(3) Å, Table 2), and their shortening and equalization (1.753(3) and 1.742(3) Å) is also observed in **Na$_2$**-*anti*-**IIDBT**. The two-fold reduction leads to the shortening of the C1′-C14 and C12-C13 bonds (1.399(4) and 1.405(4) Å) and elongation of the C5-C12 and C13-C14 bonds (1.409(4) and 1.380(4) Å), which all fall into the aromatic bond length range. Interestingly, these bond length changes for *syn*- and *anti*-**IIDBT** are nicely reproduced by calculations (Figures S9–S10). Furthermore, the core geometry changes of *syn*-**IIDBT** and *anti*-**IIDBT** upon reduction can be illustrated by selected dihedral angles in comparison to the corresponding neutral states (see more details in Table S2).

In **Na**-*syn*-**IIDBT**, the counterions are packed unidirectionally through C–H···π interactions between *syn*-**IIDBT** monoanions and the 18-crown-6 and THF molecules from the adjacent cationic moieties, with the shortest distances ranging from 2.545(7) to 2.806(7) Å (Figure 2a). In **Na$_2$**-*syn*-**IIDBT**, the ionic moieties are stacked into 1D columns through C–H···π contacts between *syn*-**IIDBT**$^{2-}$ and 18-crown-6 (2.550(9)–2.607(9) Å), and those columns are further linked into a 2D network with a rotation angle of 180° (2.729(9) Å, Figure 2b). In the packing of **Na$_2$**-*anti*-**IIDBT**, the counterions are stacked based on the C–H···π interactions (2.349(5)–2.801(5) Å) between the *anti*-**IIDBT**$^{2-}$ anions and 18-crown-6 from the neighboring cationic moieties to form a 2D layer (Figure 2c).
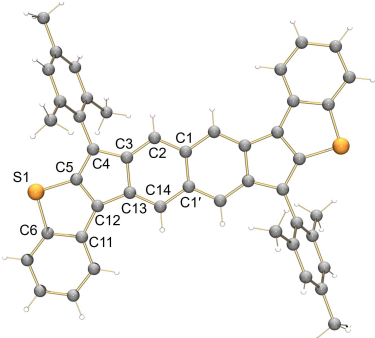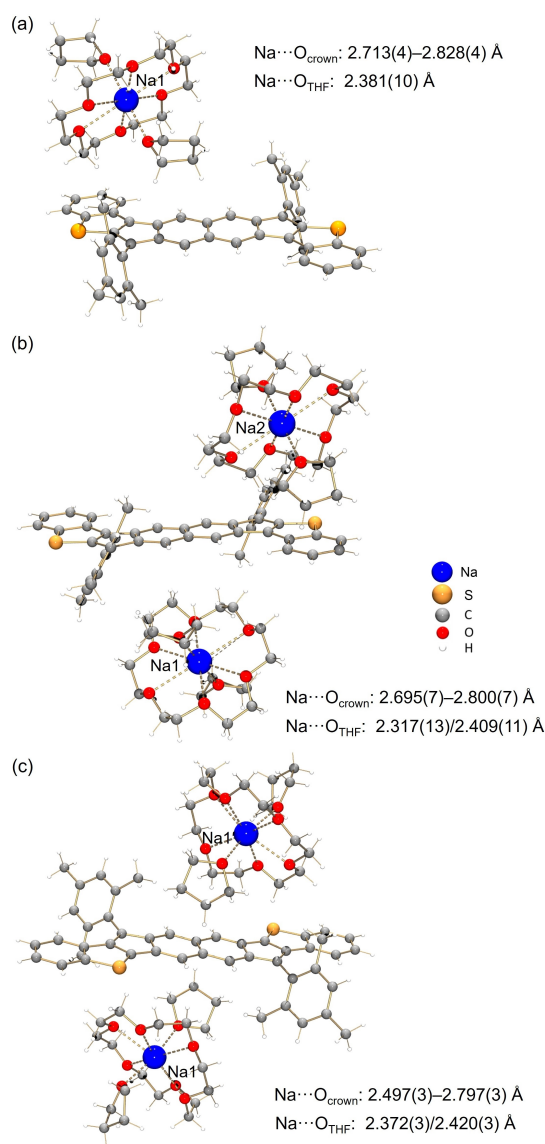

Figure 1. Crystal structures of (a) **Na**-*syn*-**IIDBT**, (b) **Na$_2$**-*syn*-**IIDBT**, and (c) **Na$_2$**-*anti*-**IIDBT** (ball-and-stick models).[26] The Na–O distances are consistent with literature values.[27]

Overall, the structural changes of *syn*-**IIDBT** and *anti*-**IIDBT** upon mono-reduction mainly occur on the central naphthalene core, which loses the partial quinoidal-like character and becomes more aromatic; furthermore, re-aromatization is found in the thiophene unit in both dianions. The S-shape distortion from the center to the sides of the molecules is observed in both neutral forms, which becomes more pronounced in **Na$_2$**-*syn*-**IIDBT** but less evident in **Na$_2$**-*anti*-**IIDBT**.
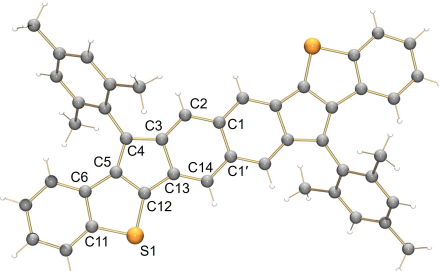
Joint evaluation of the electronic structure of the neutral and monoradicals (charged radicals): Molecular orbital mixing

Spin polarization[28] effects are essential to correctly describe the physics and chemistry of molecular species featuring

Table 1. Key bond distances (Å) of neutral *syn*-IIDBT, Na-*syn*-IIDBT, and Na$_2$-*syn*-IIDBT, along with the labelling scheme.

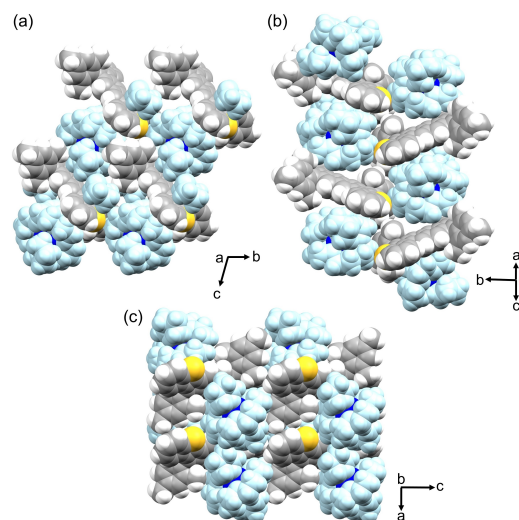| Bond	*syn*-IIDBT[a]	Na-*syn*-IIDBT	Na$_2$-*syn*-IIDBT
S1–C5	1.731(3)	1.751(5)	1.747(7)
S1–C6	1.753(4)	1.764(5)	1.756(8)
C1–C1′	1.446(6)	1.445(9)	1.450(13)
C1–C2	1.401(4)	1.402(6)	1.398(8)
C1′–C14	1.425(4)	1.416(6)	1.402(9)
C2–C3	1.386(5)	1.387(6)	1.382(9)
C3–C4	1.419(4)	1.434(6)	1.471(9)
C3–C13	1.464(4)	1.454(6)	1.461(9)
C4–C5	1.425(5)	1.407(7)	1.400(10)
C5–C12	1.399(5)	1.405(7)	1.410(10)
C6–C11	1.422(5)	1.424(6)	1.422(10)
C11–C12	1.431(5)	1.418(6)	1.425(10)
C12–C13	1.450(5)	1.428(6)	1.446(9)
C13–C14	1.361(5)	1.376(6)	1.379(9)

[a] Ref. [23].

Table 2. Key bond distances (Å) in neutral *anti*-IIDBT and Na$_2$-*anti*-IIDBT, along with the labeling scheme.

Bond	*anti*-IIDBT[a]	Na$_2$-*anti*-IIDBT
S1–C11	1.760(3)	1.753(3)
S1–C12	1.716(3)	1.742(3)
C1–C1′	1.457(5)	1.461(6)
C1–C2	1.398(4)	1.413(4)
C1′–C14	1.420(4)	1.399(4)
C2–C3	1.387(4)	1.381(4)
C3–C4	1.424(4)	1.431(4)
C3–C13	1.463(3)	1.471(4)
C4–C5	1.426(4)	1.417(4)
C5–C6	1.441(4)	1.452(4)
C5–C12	1.395(4)	1.409(4)
C6–C11	1.416(4)	1.423(5)
C12–C13	1.438(4)	1.405(4)
C13–C14	1.364(4)	1.380(4)

[a] Ref. [22].

Figure 2. Solid-state packing of (a) Na-*syn*-IIDBT, (b) Na$_2$-*syn*-IIDBT, and (c) Na$_2$-*anti*-IIDBT (space-filling models). {Na$^+$(18-crown-6)(THF)$_2$} moieties and interstitial THF molecules are shown in different shades of blue.

diradicals can be introduced via configuration interaction calculations.[29] A cost-effective alternative relies on the use of unrestricted DFT calculations providing broken symmetry (BS) molecular orbitals. Indeed, BS-UDFT[30] on OS diradicals provide a more accurate representation than restricted CS counterparts and include the spin polarization effects. Spin polarization might also affect single radical species derived from the OS neutral species. To quantify spin polarization in all these species one should determine the changes in unrestricted BS molecular orbitals with respect to the CS (restricted DFT) counterparts. In fact, it is well known that BS orbitals can be represented as linear combinations of CS orbitals.[31] Following this strategy, we determined the orbital mixing for neutral diradicals and charged radicals computed at UDFT level with respect to the corresponding set of CS orbitals.

The orbital energy of both CS (thin lines) orbitals (B3LYP/6-311G*) and BS (thick lines) for the different neutral species are shown in Figure 3 as a function of the diradical character descriptor, y_0 (PUHF).[14,31] The OS species displays a larger orbital energy gap than the CS ones in account of the stabilized neutral diradical configuration. Similar results are obtained as a function of PUB3LYP y_0 values[32] in Table 3 (see Figures S11, S12

Table 3. Intramolecular reorganization energies $\lambda_i(BS)$ and $\lambda_i(CS)$ in eV associated with hole and electron transfer for BT and B derivatives.

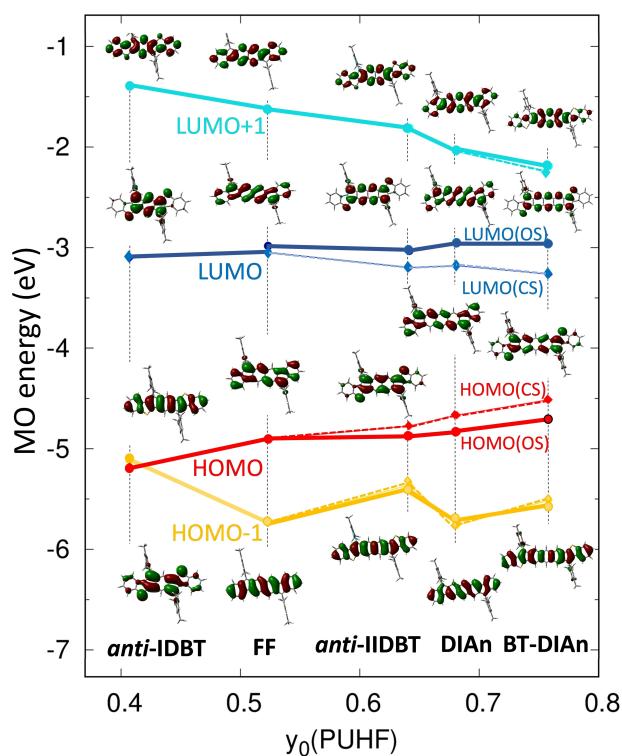| Molecule	y_0(PUHF) 6-311G*	Hole transport $\lambda_i(BS)$ $[\lambda_i(CS)]$	Electron transport $\lambda_i(BS)$ $[\lambda_i(CS)]$
anti-IDBT	0.407	– [0.204]	– [0.131]
anti-IIDBT	0.641	0.148 [0.219]	0.100 [0.086]
BT-DIAn	0.758	0.086 [0.175]	0.113 [0.073]
FF	0.523	0.147 [0.227]	0.158 [0.219]
DIAn	0.681	0.069 [0.189]	0.104 [0.169]
syn-IDBT	0.432	– [0.285]	– [0.197]
syn-IIDBT	0.691	0.126 [0.194]	0.078 [0.088]

unpaired electrons and reveal the importance of electron correlation. Accordingly, double spin polarization effects in

Chemistry–A European Journal

Research Article
doi.org/10.1002/chem.202300388

Chemistry
Europe
European Chemical
Societies Publishing

Figure 3. Correlation of B3LYP/6-311G* frontier MO energies of *anti*-IDBT, **FF**, *anti*-IIDBT, **DIAn** and **BT-DIAn** as a function of y_0 (PUHF). Filled rhombuses/circles correspond to CS-B3LYP/6-311G*/BS-UB3LYP/6-311G* energies.

and S13 together with RM06-2X/6-311G* calculations in Figures S14-S15).

The main trends for the computed CS/BS orbitals and energies in Figure 3 are:

(1) The most striking difference between BT and B terminations relies on the confinement of the HOMO and LUMO, either for the CS and the BS orbitals, between the sulfur atoms in the BT series (only for *anti*-isomers) which produces an effective conjugation extension that is shorter than the whole conjugated carbon skeleton. This is due to the repulsive effect of sulfur atoms.[22]

(2) HOMO/HOMO-1 orbitals are well separated in energy for the B-terminated series, an energy gap that is smaller in the BT-terminated ones with the extreme case of *anti*-IDBT where this order is inverted. This is particularly relevant as might impart unique spectroscopic features in its radical cation.

(3) LUMO/LUMO+1 orbitals are well separated in energy, showing an energy gap decrease with the extension of the conjugated core. This suggests that a similar LUMO+1/ LUMO orbital inversion as that in point (2) might occur in longer members.

(4) HOMO/LUMO orbitals are generally more uniformly delocalized over the conjugated core in B-terminated systems. Orbital mixing coefficients, computed for diradicals and charged radicals (Tables S4-S8), show that BS orbitals (neutral diradicals) are strongly mixed combinations of CS

HOMO and LUMO orbitals due to correlation effects including double spin polarization. Such HOMO-LUMO mixing becomes larger for larger diradical character, with mixing coefficients as of 0.45 (see Table S8). In contrast, the orbitals of cations and anions show large superposition with the CS orbital sets, indicating substantially reduced correlation effects in radicals compared to diradicals.

Electronic absorption spectra of the redox species of BT-terminated *anti*-IIDBT

The electronic UV-Vis absorption spectrum of neutral *anti*-IIDBT in Figure 4 shows a main absorption at 725 nm assigned by TD-UDFT calculations as the excitation to the ionic state described by the appropriate combination of the SOMO1→SOMO2 with the SOMO2→SOMO1 promotions (Figure 5). On the other hand, the absorption spectrum of the radical cation of *anti*-IIDBT in Figure 4 displays the common pattern found in these spectra of π-conjugated radical cation,[33,34] consisting in the appearance of two absorptions: in this particular case, at 733 nm in the visible region and at 1522 nm in the near-infrared interval. The 1522 nm band is assigned with TD-UDFT calculations to the $SOMO_{RC}(\alpha) \rightarrow LUMO_{RC}(\alpha)$ excitation, while that at 733 nm involves the excitation from a lower energy occupied π orbital of the conjugated core.

Conversely to the two-bands pattern in the radical cation, the spectrum of the radical anion of *anti*-IIDBT in Figure 4 only
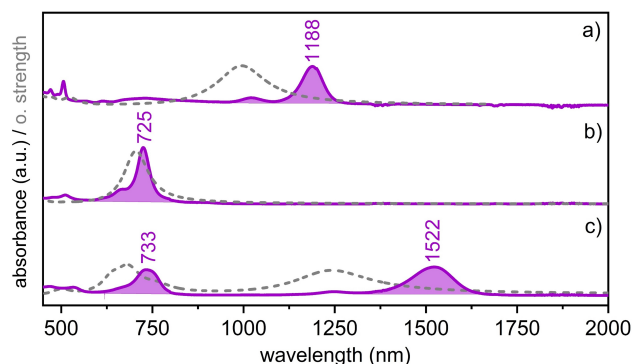

Figure 4. Pink solid lines: UV-Vis-NIR absorption spectra of 10^{-4} M of the radical anion (a), neutral (b), and radical cation (c) of *anti*-IIBDT. The redox species are obtained upon electrolysis in CH_2Cl_2/0.1 M Bu_4NPF_6. Gray broken lines correspond to the TD-UB3LYP/6-311G* computed spectra.
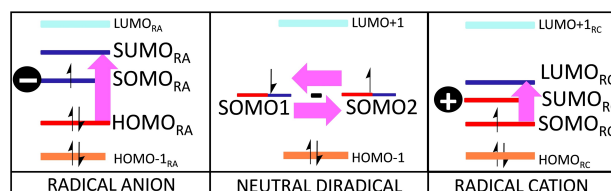

Figure 5. Representation of the electronic excitations (pink arrows) dominating the lowest energy bands in the spectra of neutral diradical, radical cation and radical anion. Orbital labels are according to Scheme 2.

Chemistry–A European Journal

Research Article
doi.org/10.1002/chem.202300388

Chemistry
Europe
European Chemical
Societies Publishing

has one main NIR band at 1188 nm, which is assigned by TD-UDFT to the HOMO$_{RA}$(β)→SUMO$_{RA}$(β) excitation (see Figure 5 and Scheme 2).[35,36] Hence, for a same compound, we can observe the evolution of the electronic transitions in the absorption spectra of the odd π-electron radical cation and anion relative to the parent neutral diradical precursor. The lowest energy excitations in the neutral vs. charged *anti*-IIDBT (see Figure 5) all involve the frontier orbitals around the gap with a common orbital origin although it appears, as stated, at very different energies in the three species.

Assuming that *anti*-IIDBT in its neutral diradical departs from two bonding decoupled SOMO orbitals, one-electron extraction/addition on one of these SOMOs almost restores the nature of CS delocalized orbitals (Table S5), underlying the more significant correlation effects (spin polarization) on the diradicals compared to the monoradicals. Indeed, we find that the MOs of cations and anions almost resemble those of the CS neutrals (*e.g.*, compare Figure S16 with Figure S12). Furthermore, the SOMO$_{RA}$ of the radical anion is exclusively centered in the core of *anti*-IIDBT totally excluding the external benzenes. In contrast, the SOMO$_{RC}$ of the radical cation further spreads out across the whole backbone including the terminal moieties, which, in part, explains the smaller energies for its transition compared with the more confined character of the SOMO$_{RA}$ in the anions.

Electronic absorption spectra of the redox species of the three anti isomers with BT termination

Figure 6 shows the UV-Vis-NIR absorption spectra of the cations and anions of *anti*-IDBT, *anti*-IIDBT, and BT-DIAn. We observe the same spectral pattern for the three radical ionic compounds, either cations or anions, which suggests the same assignment as those in *anti*-IIDBT. The spectral profile of the radical cation of *anti*-IDBT, however, is slightly different compared with those of the other two. The main difference consists in the larger intensity of its SOMO$_{RC}$→LUMO$_{RC}$ band at 598 nm compared with that at 1163 nm, both in *anti*-IDBT, an

effect that reverses in the larger compounds where the lowest energy NIR band becomes the strongest.

This spectral difference in the radical cation of *anti*-IDBT is readily explained by the energy inversion of HOMO/HOMO-1 orbitals (of the neutral species) discussed above (Figure 3) and supported by the predicted spectra (Figure S17). Indeed, if the theoretical electronic absorption spectrum of the radical cation of *anti*-IDBT is simulated upon extraction of the electron from the HOMO-1 orbital (instead of the HOMO), namely, the orbital displaying the same nature as the HOMO in longer compounds, it appears remarkably different from its current experimental spectrum (Figure S18) and more similar to those of the longer cations. The different orbital origin of the transition of the *anti*-IDBT cation compared to its longer BT-analogues justifies the smaller intensity of its lowest energy band which emerges as a result of the charge transfer excitation from the phenyl substituents to the conjugated core (Table S9).

The progressive energy differentiation between the SOMO$_{RC}$ of *anti*-IIDBT and BT-DIAn and their HOMO$_{RC}$ in the radical cations (Figure 7) on enlarging the π-core reflects the trend observed in Figure 3 for the neutrals. This might be attributed to the progressive increase of aromatic character on the bridge with size, reminiscent of the increasing diradical character in
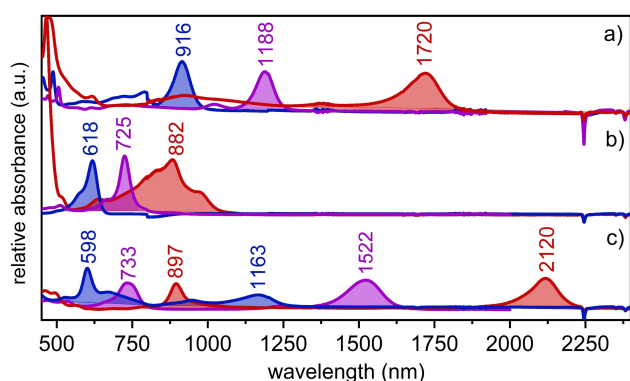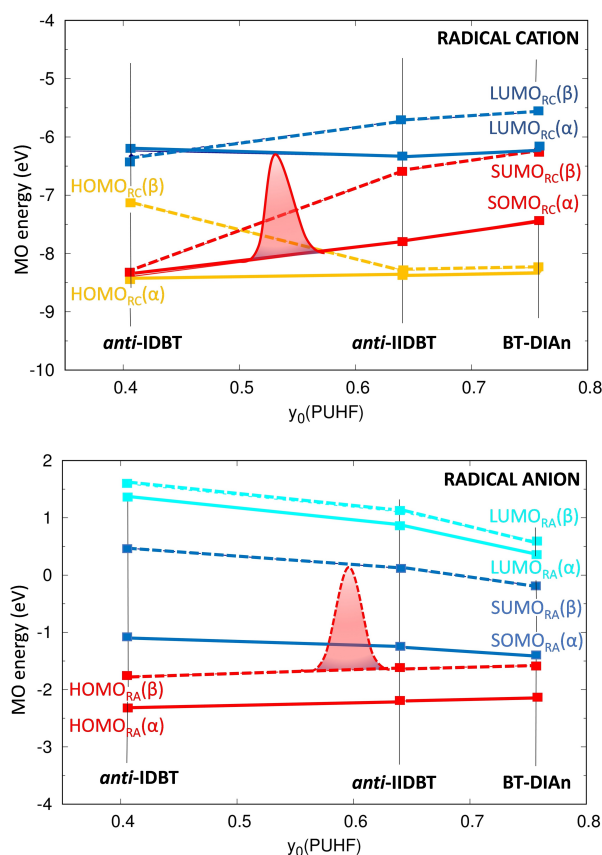

Figure 6. UV-Vis-NIR electronic absorption spectra of 10^{-4} M of the radical anions (a), neutrals (b), and radical cations (c) of *anti*-IDBT (blue), *anti*-IIDBT (purple), and BT-DIAn (red). The redox species are obtained upon electrolysis at 298 K in CH$_2$Cl$_2$/0.1 M Bu$_4$NPF$_6$.

Figure 7. DFT/UB3LYP/6-311G* orbital energies of the cations (top) and anions (bottom) of the BT- compounds. The color codes and orbital levels are in Scheme 2. Solid and dashed lines refer to α and β orbitals. Note that (*) the SUMO$_{RC}$ of IDBT corresponds to the HOMO$_{RC}$ of IIDBT and BT-DIAn. Gaussians show the lowest energy excitation.

Chemistry–A European Journal

Research Article
doi.org/10.1002/chem.202300388

Chemistry Europe
European Chemical
Societies Publishing

the neutrals. Thus, the absolute energy of the $HOMO_{RC}$ in the radical cation can be related with the aromatic character on the bridge, in such a way that the larger the aromatic character (for a given size) the smaller its absolute energy. Because the diradical character follows the trend of $y_0(anti\text{-}IDBT) < y_0(anti\text{-}IIDBT) < y_0(BT\text{-}DIAn)$, thus the aromatic character on the bridge increases in the same way and, therefore, the energy of $HOMO_{RC}$ would concomitantly decrease in absolute terms. This expectation is not fully reproduced by calculations in Figure 7 owing to the attenuation of this "aromatic" effect by the fact that the increasing number of π-electrons on enlarging the bridge size makes the energy of the occupied orbitals to be higher on going from benzene to naphthalene and to anthracene. The compensation of the two effects results in a slight increase of the absolute energy of the $HOMO_{RC}$ orbital in the series that is smaller than that undergone by the $SOMO_{RC}s$ of $anti\text{-}IIDBT$ and $BT\text{-}DIAn$, unaffected by the aromatic factor and overall resulting in a concomitant $SOMO_{RC}/HOMO_{RC}$ energy gap increase.

Conversely, in the radical anions, the $SOMO_{RA}/LUMO_{RA}$ energy difference in Figure 7 is reduced as the acene core is extended due to a faster size-dependent energy lowering of the $LUMO_{RA}$ than that of the $SOMO_{RA}$, yielding a net reduction of the energy gap.. In this regard, both the $SOMO_{RA}$ and $LUMO_{RA}$ behave as those of typical π-conjugated molecules which lower the energies of the empty orbitals with the increasing number of π-electrons (in contraposition to the energy increase of the occupied orbital). The correlation and orbital effects introduced in computed MOs and excitation energies of radical anions, neutral diradicals, and radical anions calculated at TD-UB3LYP/6-311G* level nicely account for the chain length dependence of the experimental spectra in Figure 8 (left). On the other hand, if the energies of the $SOMO_{RC}{\rightarrow}LUMO_{RC}$ bands of the radical cations and the $HOMO_{RA}{\rightarrow}SOMO_{RA}$ of the radical anions are represented as a function of the diradical index of the neutrals, in Figure 8 (right), there is a general good correlation providing slopes of 1.89 in the anions and 1.44 in the cations due to the above mentioned different π-delocalization natures.

Electronic absorption spectra of the B- and BT-terminated redox species

Figure 9 shows the electronic absorption spectra of the radical anion and cation of **FF** in comparison with those of **anti-IIDBT**. Whereas the bands in **FF** in the neutral/radical cation states are located at shorter/higher wavelength/energy than the corresponding species of **anti-IIDBT**, surprisingly, the bands of the radical anion of **FF** appear in the opposite disposition relative to those of the anion of **anti-IIDBT**. This behavior is also reproduced by theory on the redox species of **FF** and **anti-IIDBT** (Figure S19). Such as shown in Figure 3, the HOMO and LUMO electron wavefunctions of **FF** spread over the entire skeleton indicating that, either in their radical cation and anion, the terminal benzenes participate in the stabilization of the two redox species. Conversely in **anti-IIDBT**, the LUMO orbital is confined in the central part between the two five member rings. This suggests that the radical anion will not delocalize in the outermost benzenes thus its absorption bands appear at shorter wavelengths compared with those of the anion of **FF**.

Electronic absorption spectra of the redox species upon anti→syn isomerization

Figure 10 shows the UV-Vis-NIR spectra of the redox species of **anti-IIDBT** together with those of their **syn**-isomers (see these of **syn**- and **anti-IDBT** in Figure S20). In all cases, the energy maxima of the lowest energy lying bands are red-shifted on **syn-IDBT/syn-IIDBT** relative to **anti-IDBT/anti-IIDBT** parents. This trend is reproduced by calculations in Figure S21. Figure 11 compares the orbitals (neutral molecules) around the gap of **syn-IIDBT** and **anti-IIDBT**. These data reveal that the HOMO and LUMO of the **syn**-isomers spread over the entire π-skeleton, thereby extending their effective conjugation with respect to their **anti**-counterparts, which readily explains the systematic red shift in their spectra.
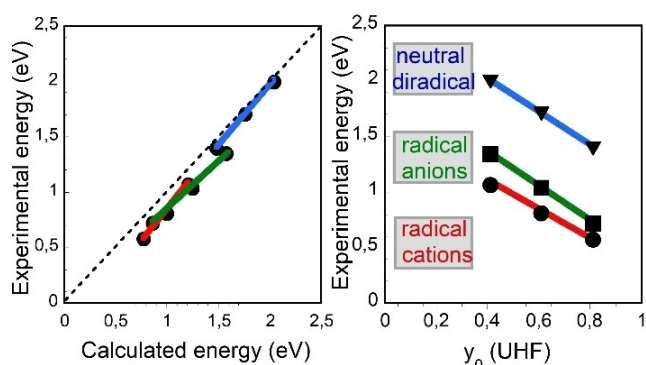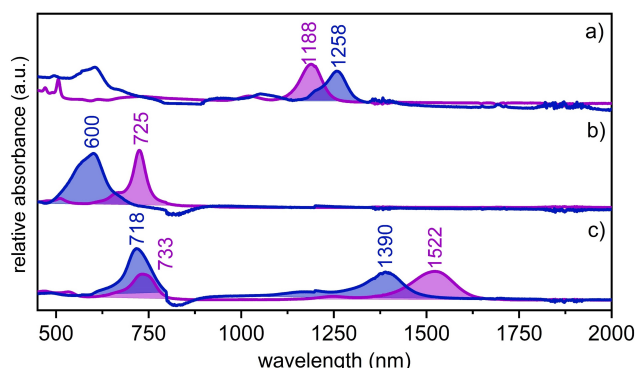

Figure 8. Left: experimental and computed excitation energies for the lowest energy absorption band of the neutral (blue), radical anions (green), and radical cations (red) of BT- derivatives. Right: the experimental energy of the same band versus y_0.

Figure 9. UV-Vis-NIR absorption spectra of 10^{-4} M solutions for the anions (a), neutrals (b) and cations (c) of **FF** (blue) and **anti-IIDBT** (purple). The redox species are obtained by electrolysis in CH_2Cl_2/0.1 M Bu_4NPF_6.
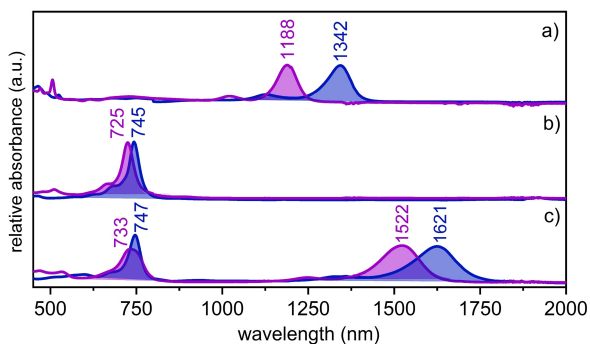
Figure 10. UV-Vis-NIR absorption spectra of 10^{-4} M solutions of the anions (a), neutrals (b), and cations (c) of *anti*-IIDBT (purple) and of *syn*-IIDBT (blue). The redox species are obtained upon electrolysis in CH_2Cl_2 / 0.1 M Bu_4NPF_6.
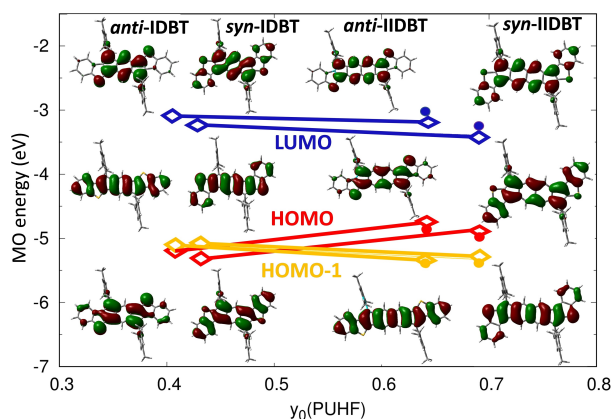

Figure 11. DFT/(U)B3LYP/6-311G* energies (eV) and orbital topologies of *anti*-IDBT, *syn*-IDBT, *anti*-IIDBT and *syn*-IIDBT isomers at the CS (rhombuses) and BS (circles) level, in the neutral state.

Intramolecular reorganization energies: impact of B and BT termination

The structural reorganization occurring upon ionization is one of the parameters connected with the efficiency of charge transport in organic semiconductors.[37,38] This is introduced in the semiclassical Marcus equation, with the λ_i parameter which modulates charge transfer rate constants of radical cations and radical anions between vicinal molecules. In this regard, it is interesting to assess interconnections between λ_i in their charged species and diradical characters.

The impact of diradical character can be assessed by comparing λ_i either assuming the CS of the neutral species (without diradical contribution), hereafter labelled $\lambda_i(CS)$ or employing the BS PES (with diradical contribution) to obtain $\lambda_i(BS)$. Both sets of λ_i generally decrease for the larger members (Table 3) partially due to the extension of the conjugated skeleton, as revealed by the $\lambda_i(CS)$ values, but is also driven by the magnitude y_0, as documented by the overall smaller values of $\lambda_i(BS)$ compared to $\lambda_i(CS)$.

Except for the smaller diradicaloids, the computed λ_i are comparable to those of best performing organic

semiconductors[38] and display well balanced values for hole and electron transfer. The λ_i values reveal significant differences: i) for B-termination, λ_i for hole and electron transports are similar, and $\lambda_i(BS)$ display a substantial reduction compared to $\lambda_i(CS)$, revealing a balanced intramolecular ambipolar character reinforced by the diradical contribution. BT-*anti*-conformers display a similar trend for hole transfer, with $\lambda_i(CS)$ larger than $\lambda_i(BS)$ and an unexpected opposite trend for electron transfer, with $\lambda_i(BS)$ larger than $\lambda_i(CS)$. Nonetheless, λ_i are small for BT-derivatives in line with the B- ones pointing out to be promising for ambipolar charge transfer. The unusual trend in $\lambda_i(BS)$ for electron transport, larger than $\lambda_i(CS)$, can be rationalized by considering the non-bonding nature of the $SOMO_{RA}$ as compared to the $SOMO_{RC}$ (Figure S16). Because the $SOMO_{RA}$ of the anion is essentially identical to the LUMO of the CS predicted geometry, its non-bonding character implies little geometry changes upon charging and therefore small $\lambda_i(CS)$ values (0.086 and 0.073 eV for *anti*-IIDBT and **BT-DIAn**, respectively). This demonstrates that beside the magnitude of diradical character, also the nature of the $SOMO_{RA/RC}$ orbital for the ions controls the magnitude of intra-molecular charge transport parameters. Interestingly, such small reorganization energies are consistent with the reported ambipolar character of **DIAn**.[15]

Description in terms of valence canonical forms, VB

In the VB context, the observed behavior of the optical spectra of the redox species of *anti*-IIDBT can be addressed assuming that in its radical anion the main VB canonical form (I_{RA} in Scheme 3) is the form with the negative charge on the apical carbons of the five-membered rings. This form is dominant since: (i) the electron-rich sulfur atom, which repels the negative charge pushing it to resonate through the central π-core; and (ii) aromatic character of the central acene core which prevents charge delocalization. The degree of localization in this I_{RA} is confirmed by the S1-C12 and C3-C4 bond length increments in Table 1 in the dianion of *anti*-IIDBT compared to the neutral. In the radical cation, however, the electron-rich nature of the sulfur permits delocalization of the positive charge, hence blocking further resonance towards the ends (see I_{RC} and II_{RC} forms in Scheme 3). In any of the two types of ions, the thiophenes impede delocalization on the peripheral benzenes, with a greater localization effect in the anion forcing the relevant optical bands at larger energies.

In the VB context, cross-conjugation of sulfur regarding the apical carbon radicals of *syn*-IIDBT (Scheme 3) accounts for the spectral evolution in the redox states. In the anion of *syn*-IIDBT, there are two resonance forms, II_{RA} and III_{RA} that similarly cross-conjugate sulfur and negative charge whereas in the anion of *anti*-IIDBT it is the VB form, I_{RA}, that puts in linear conjugation the sulfur/charge interaction. This accounts for the red-shifts of the electronic absorption bands in the cross-conjugated systems or on *anti*-IIDBT→*syn*-IIDBT. The similar contributions of forms II_{RA} and III_{RA} in the anion of *syn*-IIDBT is revealed by the length equalization of its C4-C5 and C5-C12 bond distances,
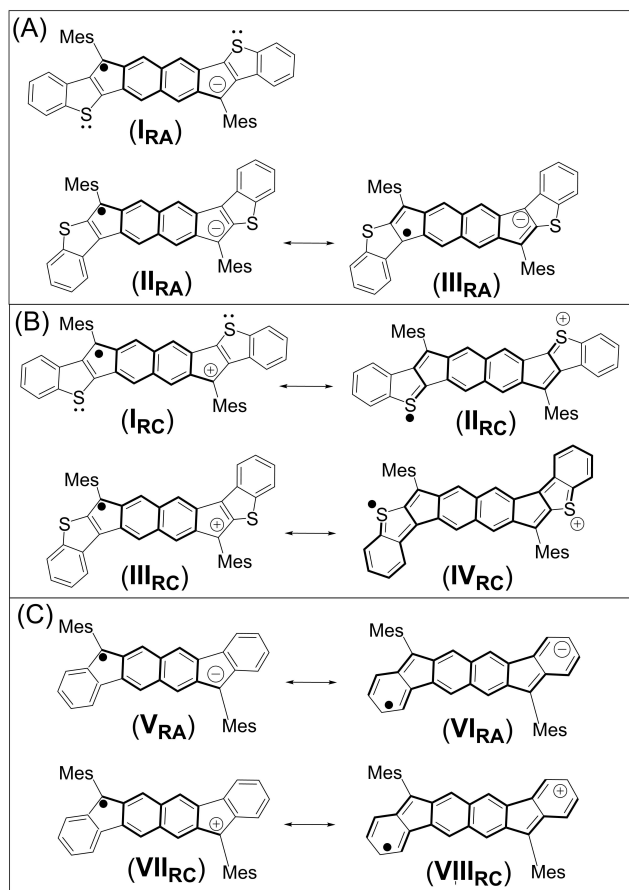
Scheme 3. VB canonical forms of the anions of *anti*-IIDBT and *syn*-IIDBT (A), for cations (B), and the same for **FF** (C).

1.407(7) and 1.405(7) Å regarding the same bond distances, 1.425(5) and 1.399(5) Å in the neutral (Table 1). In the cation of *syn*-**IIDBT** the resonance of the positive charge in the sulfur atom implies the rupture of the aromaticity of the external benzene (form IV_{RC} in Scheme 3) which simultaneously provokes a larger π-electron delocalization over the whole conjugated path and the red-shifts of the electronic bands in the cation of *syn*-**IIDBT** compared to those of the cation of *anti*-**IIDBT**.

In the case of **FF** in Scheme 3 the main VB forms of the two redox species are V_{RA} and VII_{RC} which get confined to the apical carbons (blockade effect of the aromatic benzenes surrounding it). In the anion of **FF**, delocalization of the negative charge in the external aromatic benzenes seems more feasible (VI_{RA}) than in the anion of *anti*-**IIDBT** through the thiophene ring (i.e., electronic bands are red-shifted in the anion of **FF**). Interestingly, repulsion of the sulfur towards the negative charge is seemingly more effective to impede its resonance over the external benzenes than the aromatic units in **FF**. The situation is reversed in the cations where the thiophenes strongly favor cation delocalization.

Conclusions

For the study of small-medium diradical character in molecular hydrocarbons, molecular orbital theory based on unrestricted DFT becomes very suitable since electron correlation and spin polarization can be easily considered. Here, we systematically address this problem of electron correlation in a series of neutral diradicals and monoradical charged ions based on the indaceno platform derivatized with benzothiophenes and with isomerization. We found out that in the anions and cations the effects of electron correlation and spin polarization are largely mitigated. The evolution of optical properties of all these redox species have been addressed in terms of their molecular orbital properties and also in the context of the valence bond theory, providing a unified and inter-connected description. In our case, all optical properties are accounted by within the MO picture, while the X-ray structures obtained for some of the radical anions are straightforwardly accounted by the VB description. For the radical anions and cations, we further assess the efficiency of charge transport. Indeed, the computed reorganization energies highlight a potentially efficient ambipolar transport for most of these diradicals, as previously demonstrated for **DIAn**.[15]

The joint effort here to account for molecular properties of complex systems with strong electronic correlation in a common discussion provides a general template that will benefit scientists of different disciplines to better understand the unique properties of diradicals and monoradicals.

Conflict of Interest

The authors declare no conflict of interest.

Data Availability Statement

The data that support the findings of this study are available from the corresponding author upon reasonable request.

Chemistry–A European Journal

Research Article
doi.org/10.1002/chem.202300388

Chemistry Europe
European Chemical
Societies Publishing

[1] J. L. Bredas, G. B. Street, *Acc. Chem. Res.* **1985**, *18*, 309–315.
[2] a) B. Lüssem, C. M. Keum, D. Kasemann, B. Naab, Z. Bao, K. Leo, *Chem. Rev.* **2016**, *116*, 13714–13751.
[3] L. M. Tolbert, *Acc. Chem. Res.* **1992**, *25*, 561–568.
[4] L. M. Tolbert, X. Zhao, *J. Am. Chem. Soc.* **1997**, *119*, 3253–3258.
[5] A. Facchetti, Y. Deng, A. Wang, Y. Koide, H. Sirringhaus, T. J. Marks, R. H. Friend, *Angew. Chem. Int. Ed.* **2000**, *39*, 4547–4551; *Angew. Chem.* **2000**, *112*, 4721–4725.
[6] J. C. Ribierre, T. Fujihara, S. Watanabe, M. Matsumoto, T. Muto, A. Nakao, T. Aoyama, *Adv. Mater.* **2010**, *22*, 1722–1726.
[7] K. Takahashi, K. Matsuoka, T. Takimiya, Y. A. Otsubo, *J. Am. Chem. Soc.* **2005**, *127*, 8928–8929.
[8] J. Casado, L. L. Miller, K. R. Mann, T. M. Pappenfus, H. Higuchi, E. Orti, B. Milián, R. Pou-Amérigo, V. Hernandez, J. T. López Navarrete, *J. Am. Chem. Soc.* **2002**, *124*, 12380–12388.
[9] F. Liu, G. L. Espejo, S. Qiu, M. M. Oliva, J. Pina, J. S. Seixasde Melo, J. Casado, X. Zhu, *J. Am. Chem. Soc.* **2015**, *137*, 10357–10366.
[10] C. Zhang, S. Medina Rivero, W. Liu, D. Casanova, X. Zhu, J. Casado, *Angew. Chem. Int. Ed.* **2019**, *58*, 11291–11295; *Angew. Chem.* **2019**, *131*, 11413–11417.
[11] L. Yuan, D. Huang, S. Medina Rivero, A. Carreras, C. Zhang, Y. Zou, X. Jiao, C. R. McNeill, X. Zhu, C. Di, D. Zhu, D. Casanova, J. Casado, *Chem* **2019**, *5*, 964–976.
[12] L. Yuan, W. K. Heng, B. S. Lee, N. Aratani, J. L. Zafra, N. Bao, R. Lee, Y. M. Sung, Z. Sun, K. W. Huang, R. D. Webster, J. T. L. Navarrete, D. Kim, A. Osuka, J. Casado, J. Ding, J. Wu, *J. Am. Chem. Soc.* **2012**, *134*, 14913–14922.
[13] S. R. González, Y. le, Y. Aso, J. T. López Navarrete, J. Casado, *J. Am. Chem. Soc.* **2011**, *133*, 16350–16353.
[14] M. Nakano, B. Champagne, *J. Phys. Chem. Lett.* **2015**, *6*, 3236–3256.
[15] G. E. Rudebusch, J. L. Zafra, K. Jorner, K. Fukuda, J. L. Marshall, I. Arrechea-Marcos, G. L. Espejo, C. J. Ponce-Ortiz, C. J. Gomez-Garcia, L. N. Zakharov, M. Nakano, H. Ottosson, J. Casado, M. M. Haley, *Nat. Chem.* **2016**, *8*, 753–759.
[16] T. Jousselin-Oba, M. Mamada, J. Marrot, A. Maignan, C. Adachi, A. Yassar, M. Frigoli, *J. Am. Chem. Soc.* **2019**, *141*, 9373.
[17] H. K. Kubo, M. Chikamatsu, R. Azumi, J. Tsutsumi, K. Ogawa, W. Yamane, T. Nishiuchi, T. Kubo, T. Hasegawa, K. Kanai, *Adv. Funct. Mater.* **2016**, *26*, 277–283.
[18] Y. Ni, T. Y. Gopalakrishna, H. Phan, T. S. Herng, S. Wu, Y. Han, J. Ding, J. Wu, *Angew. Chem. Int. Ed.* **2018**, *57*, 9697–9701; *Angew. Chem.* **2018**, *130*, 9845–9849.
[19] D. T. Chase, B. D. Rose, S. P. McClintock, L. N. Zakharov, M. M. Haley, *Angew. Chem. Int. Ed.* **2011**, *50*, 1127–1130; *Angew. Chem.* **2011**, *123*, 1159–1162.
[20] A. S. Hacker, M. Pavano, J. E. Wood, H. Hashimoto, K. M. D'Ambrosio, C. K. Frederickson, J. L. Zafra, C. L. Gómez-García, V. Postils, A. R.

McDonald, D. Casanova, D. K. Frantz, J. Casado, *Chem. Commun.* **2019**, *55*, 14186–14189.
[21] J. J. Dressler, A. C. Valdivia, R. Kishi, G. E. Rudebusch, A. M. Ventura, B. E. Chastain, C. J. Gómez-García, L. N. Zakharov, M. Nakano, J. Casado, M. M. Haley, *Chem* **2020**, *6*, 1353–1368.
[22] J. J. Dressler, M. Teraoka, G. Espejo, R. Kishi, S. Takamuku, C. J. Gómez-García, L. N. Zakharov, M. Nakano, J. Casado, M. M. Haley, *Nat. Chem.* **2018**, *10*, 1134–1140.
[23] J. E. Barker, J. J. Dressler, A. C. Valdivia, R. Kishi, E. T. Strand, L. N. Zakharov, S. N. MacMillan, C. J. Gómez-García, M. Nakano, J. Casado, M. M. Haley, *J. Am. Chem. Soc.* **2020**, *142*, 1548–1555.
[24] T. A. Albright, J. K. Burdett, M. H. Whangbo, *Orbital Interactions in Chemistry, Second Edition*, John Willey and Sons, Hoboken, New Jersey, **2013**.
[25] S. S. Shaik, P. C. Hiberty, *A Chemist's Guide to Valence Bond Theory.* Wiley-Interscience: New Jersey, **2018**.
[26] Deposition Numbers 2210279, 2210280, and 2210281 contain the supplementary crystallographic data for this paper. These data are provided free of charge by the joint Cambridge Crystallographic Data Centre and Fachinformationszentrum Karlsruhe Access Structures service.
[27] a) A. V. Zabula, S. N. Spisak, A. S. Filatov, V. M. Grigoryants, M. A. Petrukhina, *Chem. Eur. J.* **2012**, *18*, 6476–6484; b) S. N. Spisak, Z. Wei, A. Yu. Rogachev, T. Amaya, T. Hirao, M. A. Petrukhina, *Angew. Chem. Int. Ed.* **2017**, *56*, 2582–2587; *Angew. Chem.* **2017**, *129*, 2626–2631.
[28] a) *Diradicals* (Ed.: W. T. Borden) Wiley, New York, **1982**. b) M. Abe, *Chem. Rev.* **2013**, *113*, 7011–7088.
[29] M. Be Amor, *J. Chem. Phys.* **2020**, *153*, 044118-1-044118-12.
[30] J. Gräfenstein, E. Kraka, M. Filatov, D. Cremer, *J. Mol. Sci.* **2002**, *3*, 360–394.
[31] K. Yamaguchi, *Chem. Phys. Lett.* **1975**, *33*, 330–335.
[32] S. Canola, J. Casado, F. Negri, *Phys. Chem. Chem. Phys.* **2018**, *20*, 24227–24238.
[33] E. E. Havinga, J. L. van Donger, R. A. J. Janssen, J. Cornil, J. L. Brédas, *Chem. Eur. J.* **1998**, *4*, 1509–1522.
[34] S. Barlow, C. Risko, S. A. Odom, S. Zheng, V. Coropceanu, L. Beverina, J. L. Brédas, S. R. Marder, *J. Am. Chem. Soc.* **2012**, *134*, 10146–10155.
[35] H. Hayashi, J. E. Barker, A. Cárdenas Valdivia, R. Kishi, S. N. MacMillan, C. J. Gómez-García, H. Miyauchi, Y. Nakamura, M. Kato, M. M. Haley, J. Casado, *J. Am. Chem. Soc.* **2020**, *142*, 20444–20455.
[36] G. E. Rudebusch, G. Z. Espejo, J. L. Zafra, M. Pena-Alvarez, S, N, Spisak, K. Fukuda, Z. Wei, M. Nakano, M. A. Petrukhina, J. Casado, M. M. Haley, *J. Am. Chem. Soc.* **2016**, *138*, 12648–12654.
[37] J. L. Brédas, D. Beljonne, V. Coropceanu, J. Cornil, *Chem. Rev.* **2004**, *104*, 4971–5004.
[38] V. Coropceanu, J. Cornil, D. A. da Silva Filho, Y. Olivier, R. Silbey, J. L. Brédas, *Chem. Rev.* **2007**, *107*, 926–952.

RESEARCH ARTICLE

Monoradical cations and anions made by redox electron transfer on neutral diradicals and both with different sign charges stabilized in an identical π-conjugated platform are understood from a dual perspective as provided by molecular orbital theory and valence bond theory. Their solid-state structures and optical properties as well as their validity for ambipolar charge transport are discussed.

RADICAL ANION

DIRADICAL

RADICAL CATION
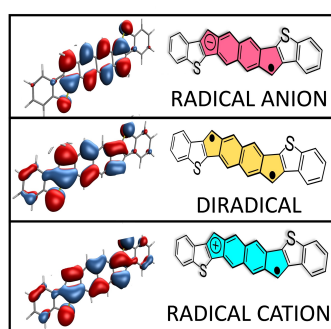
A. C. Valdivia, Y. Dai, F. Rambaldi, Dr. J. E. Barker, Dr. J. J. Dressler, Dr. Z. Zhou, Y. Zhu, Dr. Z. Wei, Prof. M. A. Petrukhina*, Prof. M. M. Haley*, Prof. F. Negri*, Prof. J. Casado*

Orbital Nature of Carboionic Mono-radicals Made from Diradicals